SILESIAN UNIVERSITY OF TECHNOLOGY PUBLISHING HOUSE

SCIENTIFIC PAPERS OF SILESIAN UNIVERSITY OF TECHNOLOGY 2025
ORGANIZATION AND MANAGEMENT SERIES NO. 241

APPLICATION OF CONVOLUTIONAL NEURAL NETWORKS FOR WINDTHROW AND WINDBREAK TIMBER VOLUME ESTIMATION IN THE STARE JABLONKI FOREST DISTRICT

Krzysztof NAJMAN[1*], Dominik MIELCZAREK[2]

[1] University of Gdansk, Faculty of Management; krzysztof.najman@ug.edu.pl, ORCID: 0000-0003-4106-2964
[2] Centrum Badawczo-Rozwojowe OPEGIEKA; dominikm.@opegieka.pl
* Correspondence author

Purpose: The study aims to estimate the volume of windfall timber using convolutional neural networks. The focus of the study centres on several key challenges in assessing the aftermath of wind damage to forests. This includes accurate quantification and volume measurement of densely downed trees, correct detection of log masks to determine their surface area and then volume, as well as revenue estimation based on wood composition variances and fluctuations in the prices of specific tree species. This capability enables forestry managers to conduct rapid financial impact assessments, crucial for insurance claims and operational budgeting. The goal is to determine whether detailed information on tree-level wind damage can be obtained using aerial imagery. The Methods section outlines the implementation of predefined objectives and assumptions. From a business perspective, the automation of this process significantly reduces the time and cost of traditional ground surveys, improving operational efficiency. The impact of hyperparameter selection on the performance and effectiveness of the resulting model was analysed. The stages of the model's training and refinement to its optimal form have been described. The detection model's effectiveness was evaluated using detection model performance indicators. A reliable, automated estimation system enhances supply chain planning for wood processing mills by providing early and accurate data on available raw material volume and quality. The article concludes with an analysis of volume and revenue estimates for a sample area in the Stare Jabłonki Forest District. Calculations of potential revenue from windthrows was performed. This directly supports strategic decision-making, allowing for optimized timber sales scheduling to capitalize on favorable market prices for specific species or grades. The estimation of potential revenue was carried out taking tree species and timber grades into account, using a detailed timber price list published by the forest districts. Ultimately, this technology transforms aerial data into a actionable business intelligence tool for revenue forecasting and resource management following disruptive natural events.

Design/methodology/approach: The study used aerial imagery acquired from two forest districts - Dobrocin and Stare Jabłonki - using a Riegl 1560i-DW II LiDAR scanner and a 150 MP RGB camera. A dataset of 538 images containing 2160 annotated logs was prepared. Detection was performed using a Mask R-CNN model based on the ResNet-101 backbone and Feature Pyramid Network (FPN) architecture. The model was trained and validated on data representing different stand densities and windthrow concentrations. Model performance was

evaluated using Precision, Recall, F1-score, and Intersection over Union (IoU) metrics. Estimated timber volumes were compared with reference data and used for potential revenue estimation according to detailed timber price lists published by the forest districts.
Findings: The model achieved high detection accuracy. The Pearson correlation coefficient between the predicted and reference values ranged from 0.96 to 0.97, and the average F1-score reached 0.766. The highest accuracy was achieved for low IoU thresholds (0.1-0.5). The difference between the estimated and actual timber volume amounted to 354 m³, and the mean estimation error for potential revenue was 7.13%.
Research limitations/implications: The main limitations of the study arise from manual data labeling and the limited sample size in areas with high tree density. The model occasionally splits long logs into several parts. Future research should expand the dataset to include more diverse examples and apply Explainable AI (XAI) methods to improve interpretability and transparency of results.
Practical implications: The use of convolutional neural networks for aerial image analysis enables fast and accurate estimation of windfall timber volume. This approach can significantly support forest management operations, improve post-storm planning efficiency, and provide rapid economic assessments before the wood loses its industrial value.
Social implications: Rapid and accurate assessment of windstorm damage supports effective forest management, reduces economic and environmental losses, and strengthens adaptive measures against climate change impacts.
Originality/value: This study presents a novel application of **Mask R-CNN convolutional neural networks** for precise estimation of windthrow timber volume based on aerial imagery. The results demonstrate the potential of artificial intelligence methods in forestry for automatic damage assessment, resource planning, and revenue forecasting.
Keywords: Disaster management, Deep learning, Instance segmentation, Timber volume.
Category of the paper: Research paper.

1. Introduction

The study aim entails an attempt to estimate the volume of windfall timber, using selected artificial intelligence methods. The implementation of a project involving estimation of timber volume has been motivated by the growing number of windstorm disasters in Poland. Wind disturbance is a worldwide issue. In the Amazon rainforest, wind damage, mainly caused by the growing incidence of convective winds, has become one of the greatest negative impacts. Strong wind is responsible for 50% of all tree mortality (Feng et al., 2023). Forest biomass plays a role in climate stability and numerous ecological processes (Pravalie et al., 2023). Throughout 2000-2021, the amount of harvested timber steadily increased. During this period, two phases were observed, characterized by an increase in the amount of harvested deadwood and windthrow. In 2021, Polish forests averaged 9.8 m^3/ha of coarse deadwood. A similar proportion was observed for dead and windfall trees, recorded at 4.9 m^3/ha. On average, every hectare of forest consists of 272 stumps in a standard distribution. Countrywide, the volume of dead coarse wood averages 9.8 m^3/ha. Half of this volume, i.e., 4.8 m^3/ha, is windfall trees

(Office of Forest Management and Geodesy)[1]. The study analyzes the case of wind damage in northern Poland, where forests have been ravaged by severe hurricanes in recent years. In 2017, the so-called 'hurricane of the century' hit the regions of the Kuyavian-Pomeranian and Pomeranian voivodeships. On August 11-12, a so-called bow echo hurricane struck, reaching speeds of up to 150km/h (Dmyterko, Bruchwald, 2020). The hurricane severely damaged a total of 39.2 thousand hectares of forest. The incidence of hurricanes in Poland shows regularity. Just a year later, in July 2018, a hurricane uprooted 10 000 trees in the Stare Jabłonki Forest District, which has been assigned the highest level of forest threat (estimated risk between 40-50%) (Dmyterko et al., 2015).

2. Natural disasters

In the face of widespread climate change awareness, a shift in approach to forest management has ensued. It has been forced by the increasing intensity and frequency of climate change-related disturbances. The consequences of these processes are difficult to predict in the long term. Authors (Filotas et al., 2014) indicate that we have been facing an unprecedented rate of abiotic changes. The new approach recognizes the uncertainty associated with environmental and social change. It promotes the view of forest management as a complex, functional network, subject to continuous and dynamic monitoring (Messier et al., 2019). These systems, used in forest planning and management, are aimed at strengthening the resilience of forests against climate change (Walker et al., 2004; Filotas et al. 2014). The sensitivity of forests to the effects of climate change can be reduced through appropriate 'forest operations' (Lindner et al., 2010). In the context of natural disasters, these measures improve the resilience of forests, counteracting the destructive effects of climate change (Seidl et al., 2014). Of importance in this context is the implementation of adaptive forestry strategies that are responsive to the ongoing climate change. Authors emphasize that the management of a forest as a complex adaptive system calls for constant monitoring of ecosystems and implementation of strategies increasing resilience to disturbances (Walker et al., 2004). The key aspect is to prevent these disturbances from affecting the ecosystem's ability to perform it basic functions. Of equal importance is the continued education of management personnel on the changing environmental conditions (Tampekis et al., 2024). Abiotic disturbances are characterized by a rapid and dynamic progression (Gieralowiec, 2020). Tree species with robust root systems are prone to breakage. Those typified by weaker root systems are more susceptible to uprooting (Krisans et al., 2020). Hurricane damage changes the landscape and reduces timber production, negatively affecting the management of forests, hydrological balance,

[1] Office of Forest Management and Forest Geodesy (2020) Guidelines for conducting a large-scale forest status survey.

and biodiversity. European forests suffer most severely due to insect infestations and plant diseases, as well as wind and wild fauna (Gardiner et al., 2013). Hurricane activity has been observed to reduce the potential for harvesting higher-grade timber (Gieralowiec, 2020). The prevalent atmospheric factors and the damage to wood limit the industrial usability of timber, which is why salvage logging operations are of such vital importance. Prompt assessment of the extent of damage allows for estimation of the workforce needed for salvage logging (Kühmaier et al., 2022). The potential for harvesting high-grade windfall and windsnap timber is also dependent on the technology and equipment utilized to harvest the timber in a given area (Gieralowiec, 2020). Windthrow stands are more susceptible to disease, given that these areas become, over time, a breeding ground for insects and fungi (Dhubháin, Farrelly, 2018). In the past, undetected clusters of uprooted trees served as breeding grounds for the bark beetle (Einzmann et al., 2017). The risk of wind damage increases proportionally to tree stand height (Zachara, 2006). A stand's susceptibility to damage is also conditional on its species composition (Zachara, 2006), soil composition, and geomorphology (Gardiner, Quine, 2020). Another factor increasing the risk of tree damage is snow cover (Heinonen et al., 2009). Recent research suggests that coniferous trees are more susceptible to wind damage than deciduous trees (Valinger, Fridman, 2021). Despite the availability of preventive measures aimed at reducing forest vulnerability to wind damage, forest managers' accountability remains limited (Zachara, 2006). The preventive measures have been conceptualized as development of logging areas narrower than 30 meters, as well as reduction of stand density by eliminating resistance points through thinning cuts. The permeability of forests reduces the risk of wind damage (Zachara, 2006). The strength and frequency of gusts are considered significant factors in terms of damage (Dhubháin, Farrelly, 2018). Stephen J. Mitchell mentions in his work the interaction of three major factors contributing to wind damage susceptibility, namely topographic exposure, soil properties and stand characteristics - the windthrow triangle (Mitchell, 1995).

3. Utilization of AI for Object Recognition

Artificial intelligence methods are employed in the modelling of phenomena when detection of patterns in data via classical statistical models proves impossible. Neural network models are increasingly utilized to solve forestry-related problems (Diez et al., 2021). Vasileios Linardos explains in his publication that the use of ML/DL algorithms allows for detection of areas affected by all types of natural disturbances (Linardos et al., 2022). Deep Learning models show great potential in estimating the risk of wind damage and assessing the extent of windthrow and windsnap damage. Artificial intelligence methods are far superior to humans in terms of data analysis speed (Sun et al., 2020). Artificial neural networks outperform such

classical statistical models as the Naive Bayes classifiers, logistic regression, support vector machines or SAMME.R in identifying areas affected by windstorm damage (Kislov, Korznikov, 2020). The advantage of such an approach lies in the automatic identification of patterns in data, without the need for feature engineering (Kislov et al., 2021). The disadvantage of using a Deep Learning model stems from its black-box nature, precluding interpretation of its performance (Cheng et al., 2022). The study involved the use of convolutional neural networks. Convolutional neural networks are a type of model tailored to structured data, e.g., images (Goodfellow et al., 2018). They are widely employed in image analysis, for such tasks as classification, detection, object recognition and semantic segmentation (Zhang et al., 2016). The neurons in convolutional neural networks are arranged three-dimensionally – by width, height, and depth, with each layer only connecting to their corresponding neurons in previous layers (O'Shea, Nash, 2015). Artificial intelligence models require vast amounts of training data, typically annotated manually by humans. Human intervention in data can input errors, potentially limiting the peak accuracy of the models (Kislov et al., 2021). Validation and correction of any manually created data by means of field measurements is recommended (Kislov et al., 2021). The advancement of artificial intelligence methods offers unprecedented opportunities in the modelling of high complex phenomena. Adaptation of these models towards solving the problems generated by natural disasters can prove beneficial to forest managers and owners (Cheng et al., 2022). Features such as precision and short lead times can play a valuable role in the planning of windstorm mitigation tasks (Sun et al., 2020). From a business perspective, the automation of this process significantly reduces the time and cost of traditional surveys, improving operational efficiency. A reliable, automated estimation system enhances supply chain planning for wood processing mills by providing early and accurate data on available raw material volume and quality.

4. Research methodology

Study area

The study utilized data on two Forest Districts - Dobrocin and Stare Jabłonki, located in Poland (Figure 1a). An analysis of the volume of windthrow and windsnap waste wood harvested in July 2018 in the Stare Jabłonki Forest District was performed. Both forest districts are geographically situated in the Warmian-Masurian Voivodeship. The Dobrocin Forest District borders the Orneta, Kudypy, Stare Jabłonki, Miłomłyn, Susz, Kwidzyn, Elbląg, and Młynary Forest Districts (Żokowski, 2023). The area of the unit extends over 842.78 km^2. The Forest District borders the Stare Jabłonki Forest District to the southeast (Figure 1b).

The area of the Stare Jabłonki Forest District totals 175.6 km^2. The dominant species in these forests are pine (79.4%), beech (7.4%), birch (6.2%), and oak (3.5%) (Przesław, 2023).

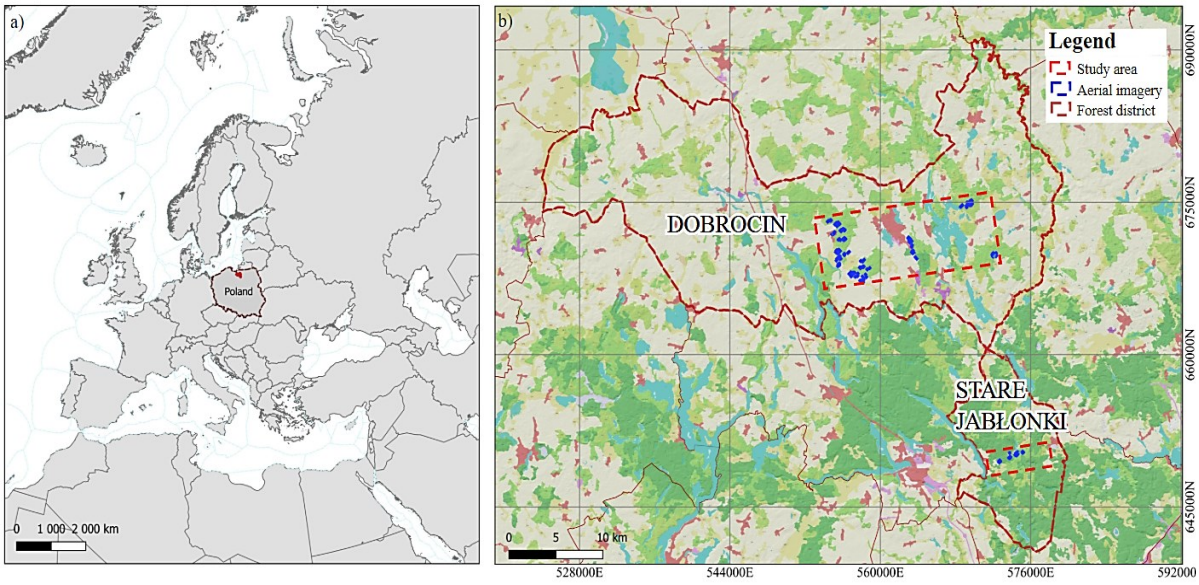

a) b)

Figure 1. Study area. Stare Jablonki, Dobrocin Forestry Districts. Information on recorded wind disturbance damage derived from the Stare Jablonki Forest District's data.

Source: own eleboration. Map generated using Land Use/Land Cover (LULC): Karra et. al., 2021.

Data collection

The Dobrocin Forest District data was collected during a leaf-off period (April), whereas the Stare Jabłonki District data – during a leaf-on period (August). Simultaneous use of data with different characteristics is assumed to affect models' ability to generalize during the processes of learning. The feature characterising the images recorded during leaf-off is the visibility of the lower strata of the stand, unobscured by tree canopy; hence, given this data, the model is expected to be more effective in detecting windthrows and debris in dense forest sections. The Stare Jabłonki District data was collected during a period of leaf cover. Despite the limited visibility of the undergrowth, downed tree boles stand out clearly against the background of dense, lush vegetation. Both data sets were acquired using a Riegl 1560i-DW II scanner in an aerial survey. The measuring device utilizes a medium-format RGB camera of 150MP resolution with a 64mm CMOS sensor. The camera is equipped with a 50 mm focal length lens. The spatial resolution was identical for both data sets. Log masks were mapped manually using QGIS 3.12 software (https://qgis.org/). Each was outlined as a polygon, rasterized and segmented into a raster mask. Using a customized Python script, the geodata was converted to the standard COCO format (Lin et al., 2014). A total of 538 images (509 x 1688 m) with 2160 downed trees marked were used in the study. Out of the entire set of images, 407 served as training data, 102 as validation data, and 32 as test data. In total, of 579 downed trees were identified and marked in the test data.

Neural Network model architecture

The Mask R-CNN model (Figure 2) consists of several stages implemented sequentially, and utilizes 63 621 918 trainable and 111 488 non-trainable parameters. The first Model block involved the use of a Feature Pyramid Network (FPN). FPNs serve to identify the input image features that allow localization of expected objects. In this stage of the model, ResNet-101 architecture, renowned for its effectiveness, was utilised (He et al., 2015).

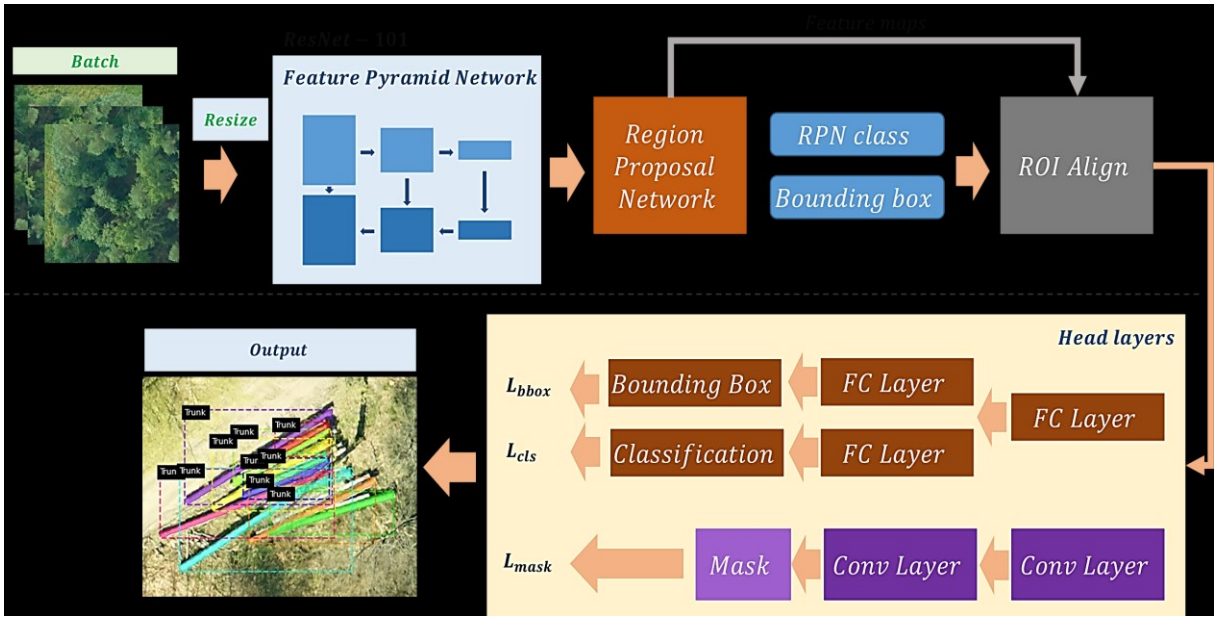

Figure 2. Diagram of MaskR-CNN model. The model consists of several sequential segments, dedicated to separate components in the task of instance detection and segmentation.

Source: a report based on: Karra et. al., 2021.

The feature pyramid outputs are fed into the next stages - Region Proposal Network (RPN) and Mask Recurrent Neural Network (MRCNN). The Region Proposal Network part conveys the layers showing proposed object locations. RPN then generates a set of predefined anchor box rectangles serving as proposed ranges within which the objects can be located. Using the anchor boxes, the model performs a regression task, indicating the area of bounding box occurrence. Correct localization of objects is achieved by the matching thereof to the areas of interest (anchor boxes). The location of potential anchor boxes is determined by the model based on the features extracted from the FPN block. Position and size errors are determined by the overlaps between the bounding boxes and the anchor boxes (based on the value of the Intersection over Union metric). Simultaneous use of anchor boxes enables identification of spatially overlapping objects. At the end of the detection process, ‘non-maximum suppression’ filtering is used in the RPN block. This process eliminates the redundant number of ranges assigned to the same object, based on the model's confidence. NMS likewise eliminates false positive indications, improving detection accuracy. The NMS function is used in RPN and MRCNN blocks to eliminate excessive bounding boxes. The process of ROI Alignment is used to extract the features characterizing the regions of interest, to predict the masks. The size of

the masks is consistent, despite the fact that bounding boxes differ in size. This is accounted for by the process of range matching performed in the ROI Align block (He et al., 2017). The function bilinearly interpolates the pixel coordinates and enables precise image masking, regardless of the size of the masked object. Each instance (bounding box) is subject to a binary mask classification by the model. The classification of masks, also known as segmentation, serves to extract a subset or uniform region from an image, based on specific properties (Stąpor, 2011). Mask R-CNN utilizes three different loss functions for each task; to classify the masks, the model calculates the average cross-entropy (Hastie et al., 2001):

$$\boldsymbol{\mathcal{L}(\Theta) = -\sum_{k=1}^{K}\sum_{i=1}^{N} y_{ik}\,\log[f_k(x_i)]} \tag{1}$$

To determine the location error limiting bounding box detection, the model calculates the smooth L_1 loss function:

$$\boldsymbol{\mathcal{L}(\Theta) = \sum_{k=1}^{K}\sum_{i=1}^{N} L_1(|y_{ik} - f_k(x_i)|)} \tag{2}$$

$$where: L_1 = \begin{cases} 0.5x^2 \; if \; |x| < 1 \\ |x| - 0.5 \; if \; |x| \geq 1 \end{cases}$$

The loss function in Eq. 2 is highly resistant to extreme outliers. Ultimately, the loss function is formulated by summing the losses from three different tasks (He et al., 2017):

$$\mathcal{L} = \mathcal{L}_{cls} + \mathcal{L}_{bbox} + \mathcal{L}_{mask} \tag{3}$$

In the above formula, $\boldsymbol{\mathcal{L}_{cls}}$ denotes the loss of classification in an instance, $\boldsymbol{\mathcal{L}_{bbox}}$ represents the bounding box position, and $\boldsymbol{\mathcal{L}_{mask}}$ signifies the loss of overlap between the predicted and reference mask. The form of the total loss function $\boldsymbol{\mathcal{L}}$ shown in Eq. (3) allows for multi-task optimization.

Training

Due to its stochastic nature, the model necessitates an iterative search for the optimal set of hyperparameters. Two phases of the model training process were planned. The first - preliminary training - was aimed at arriving at the best possible form of the weights identifying relevant image features in the Feature Pyramid Network block. The second entailed the training of remaining blocks, excluding the FPN block. This phase began with 'knowledge transfer,' i.e., the import of the weights obtained through MS COCO (Microsoft Common Objects in Context) dataset-based learning (Lin et al., 2014). The use of weights from an already trained model, capable of recognizing specific patterns in an image, was assumed to accelerate the learning process, in contrast to the learning from scratch scenario (Pi et al., 2020). All weights, except those forming part of the FPN (Feature Pyramid Network), proved trainable in the first phase of the training. Empirical observation revealed that the learning coefficient, initially set at of 0.01, caused instability during the process of model training, resulting in numerical complications. This drawback was mitigated by decrementing the learning coefficient to a value of 0.002 and employing a learning rate decay strategy, particularly the Reduce LR On Plateau technique. The weight decay (regularization) coefficient was set at 0.0005 and was not modified

throughout the entire process of the model's learning. With such an approach, loss function reductions undetected over five consecutive epochs automatically result in a downward correction of the learning coefficient's value. The correction process draws on the potential of smaller learning coefficients to aid the model's convergence through incremental adjustments, thus preventing possible instability and numerical problems potentially induced by larger steps. Systematic implementation of learning rate decay strategies, therefore, effectively optimizes the process of iterative training, ensuring a more consistent and reliable progression towards model convergence. The use of a lower coefficient value is intended to limit the impact of individual instances on the model's final decision-making capacity, thereby promoting more balanced and generalized learning. Substantial improvement in the model was observed after extending the training epochs from the initial count of 150 to 400. This extended phase of training lasted 13 hours. The training process was run using hardware equipped with two *NVIDIA GeForce GTX 1080 Ti GPUs* graphics cards of 2x11 GB memory capacity. During the initial iterations, the model showed significant susceptibility to overfitting, necessitating an expansion of the image augmentation technique repertoire. The methodological assortment was supplemented with expansion strategies, including removal of image fragments (via zero-filling) and addition of white noise. A decision was made to increase the number of validation iterations to 70, to obtain a more statistically reliable assessment of the model's actual performance. The first phase of the model training ended with an underestimation of the volume of timber, quantified at 1457 cubic meters. The model showed suboptimal performance in mask classification. In this stage of the training, the model proved highly sensitive in detection, misidentifying tree bole-like objects as downed trees. After testing, the model identified an average of 83% more uprooted trees than indicated in the ground annotations. In the second phase of the learning process, the weights in all layers were unfrozen. The process of arriving at the correct combination of parameters entailed a greater number of iterations to adjust the hyperparameters. Simultaneously, the size of the training data was gradually increased. Since the detection model employed necessitates a large amount of training data, data on both forest districts (Dobrocin and Stare Jabłonki Forest Districts) were used. The most relevant parameter modified in the second phase was the size of the generated anchor boxes. An increase in the size of the anchor boxes generated, from 256 to 512, was observed to have improved the detection of larger-sized downed trees. Subsequently, experiments were performed to assign weights to each task (mask classification and detection). Increasing in the weights of one loss function, however, compromised the learning performance in other tasks. The size of the training data in subsequent iterations was expanded by adding the instances which had posed the greatest difficulty for the model. The continuous increase in the size of the training data was instrumental in improving the model's quality. Satisfactory second-phase results were obtained after 70 epochs (over a 5-hour training process). Noteworthy is the observation that the data should be expanded to include instances of tree boles partially extending beyond the image area or partly obscured by the boles of other trees.

5. Data augmentations

To further prevent the risk of model overfitting and multiply the available data, augmentation, i.e., a series of image transformations, was used. These techniques can be categorized into two groups - radiometric transformation-related and image object geometry-related. Application of the transformation is predetermined at a certain probability, which ensures random input of data without alteration of all the data. Augmentation allows the model to expand the context contained in the data. Radiometric transformation applies to aerial images only; reference masks are not subject to such changes. To apply data augmentation, the Albumentations library (https://albumentations.ai/) was used.

Table 1.
Image transformation types. The training data generator each time modifies the data transferred to the model. Individual transformations are applied with a probability of p

Augmentation type	Transformation type	Values	p
Radiometric	*brightness modification*	$b \in [0.8, 1.0]$	0.5
	linear contrast change	$\gamma \in [0.9, 1.1]$	0.5
	Gaussian filter blurring	$\sigma \in (0, 0.1]$	0.5
Geometric	*mirror reflection*	-	0.5
	affine grid transformation	$r \in \{0, \frac{\pi}{2}, \pi, \frac{3\pi}{2}\}$	0.5
	zoom in&out	$(x, y) \in [0.8, 1.2]$	0.25
	sharpening	$\alpha_s \in (0, 0.1]$	0.25
	snowflakes	$f_z \in [0.2, 0.4]$	0.25
	coarse dropout	$s \in [0.02, 0.25]$	0.25

Source: author's own elaboration based on: https://albumentations.ai/

Training loops split the training data into batches. Batch size affects the progress of learning - a too small size can update the weights in an undesired direction, destabilizing the training process, whereas a too large size can prolong the training and prevent the model's sensitivity to rare events in data.

Analysis of the loss function curves (Figure 3), both collectively and by task, shows that the model did not lose its ability to correctly identify downed and broken trees, based on independent validation data, throughout the entire training process. The loss function values determined using the validation data are higher compared to those determined using the training data, yet the discrepancy between the two in subsequent epochs remains constant, which possibly signals an overfitting of the model.

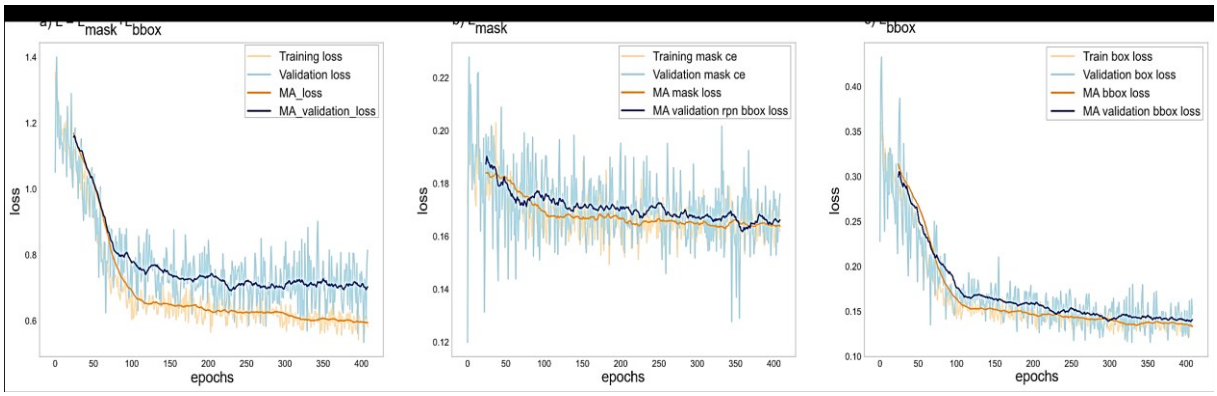

Figure 3. Different loss functions for each task. The cumulative value of the cost function consists of the sum of the loss function values determined for each discrete task. The figure shows the first stage phase of the training process.

Source: own eleboration.

Evaluation metrics

The model's effectiveness was verified using the classic indicators employed in the evaluation of classification and detection results. The model's performance was evaluated using such metrics as *Precision*, *Recall*, *F1-score*, *Average Precision (AP)* and *Intersection over Union (IoU)*. *Precision* determines the accuracy of detection:

$$Precision = \frac{TP}{TP+FP} = \frac{correctly\ predicted}{all\ predicted\ as\ positive\ instance} \tag{4}$$

$$Recall = \frac{TP}{TP+FN} = \frac{correctly\ predicted}{all\ positive\ instances} \tag{5}$$

where TP, TN, FP, and FN respectively represent true positive, true negative, false positive, and false negative indications. The overall effectiveness of the model was assessed using the *F1-score* metric, calculated as the harmonic mean of sensitivity and precision, with P_r and R_c denoting Precision and Recall, respectively (Pi et al., 2020).

$$F1 - score = \frac{1}{Pr^{-1}+Rc^{-1}} \tag{6}$$

The instances of correct object identification by the model were evaluated using *the Intersection over Union* metric. Only the cases involving *IoU* values greater than 0.1 were factored in. *Intersection over Union* (*IoU*) measures the ratio of the overlap area between the reference and predicted sets to the area of their union (Pi et al., 2020):

$$IoU = \frac{TP}{FN+FP+TP} = \frac{bbox_{predicted} \cap bbox_{reference}}{bbox_{predicted} \cup bbox_{reference}} \tag{7}$$

Average Precision (AP) is a metric widely used in detection tasks. It is calculated as the area under the precision-recall curve across all *IoU* threshold variants (ranging from 0 to 1). In the *AP* metric, r and p respectively denote recall and precision, with p_k and r_k accordingly representing the precision and recall in specific *IoU* subranges (Zhu, 2004):

$$AP = \int_0^1 p(r)dr \approx \sum_{k=1}^{n} p_k * (r_k - r_{k-1}) \tag{8}$$

Average Precision was calculated for several threshold variants k, within a defined range of $0.1 \leq k \leq 0.5$. The rationale behind such a range definition is discussed further in the article.

6. Results

Statistical evaluation

Subsequently, a prediction was performed on a pre-prepared test area, the results of which were compared against the labels of the reference data. After refining the model to a satisfactory form through training, a simulation was carried on a separate set compiled for testing purposes. A section of 10.24 ha, designated for testing, was delineated within the area of interest and divided into a grid of squares for analysis purposes. The size of a single grid cell (80 x 80 m) was dictated by the requirement to maintain the original spatial resolution – 4 cm. The analysis covered both the area directly affected by severe wind damage as well as the forest section that had withstood the force of the storm. The estimation of harvested timber volume based on annotated post-damage data provides an approximation of the actual extent of wind disturbance damage. One additional factor contributing to the uncertainty of the estimates arises from the fact that the reference data was prepared manually. Predictions were performed on the test area; for each image (i), the number of indicated uprooted trees ($\widehat{N}$) was calculated, and the volume of logs (j) from the uprooted trees ($\widehat{V}$) was estimated.

$$\widehat{N} = \sum_{i\neq 0}^{N} \sum_{j}^{M} 1_{i,IOU(j)>0.1} \tag{9}$$

To estimate the log volume, cross-sectional area A and tree length h were applied. To calculate the log length, a parallel thinning algorithm was used (Zhang, Suen, 1984).

$$\widehat{V}(m^3) = \frac{1}{d\times 10^6} \sum_{i=1}^{N} \sum_{j=0}^{M} A_{i,j} * h_{i,j} \Leftrightarrow$$
$$\frac{1}{d\times 10^6} \sum_{i=1}^{N} \sum_{j=0}^{M} [\pi * r^2]_{i,j} * h_{i,j} \tag{10}$$

On each image, the number of identifiable uprooted trees varies as M. The volume is adjusted by spatial resolution at d ≈ 4 cm. As shown in Eq. (10), the function can be rewritten as the volume of a cylinder, using the number π and the radius r.

When applied to areas of lower windthrow density, the model shows high precision. For areas of high windrow density (d > 50 trunks/100 m²), however, the model's error of underestimation gradually increases with the rising number of windrows. A strong correlation (Pearson's correlation: 0.96) between the reference and estimated counts of identified tree boles was observed. An equally strong relationship (Fig. 4) was noted between the reference and the estimated volume of logs (Pearson's correlation: 0.97). Average Precision AP, Recall, and F1 scores were calculated for all test images. The tabular summary (Table 2) shows the mean values with standard deviation, calculated for the test dataset. Logs that minimally overlap with the reference (IoU < 0.1) are not considered as identified. The results were calculated for a confidence score above 0.6.

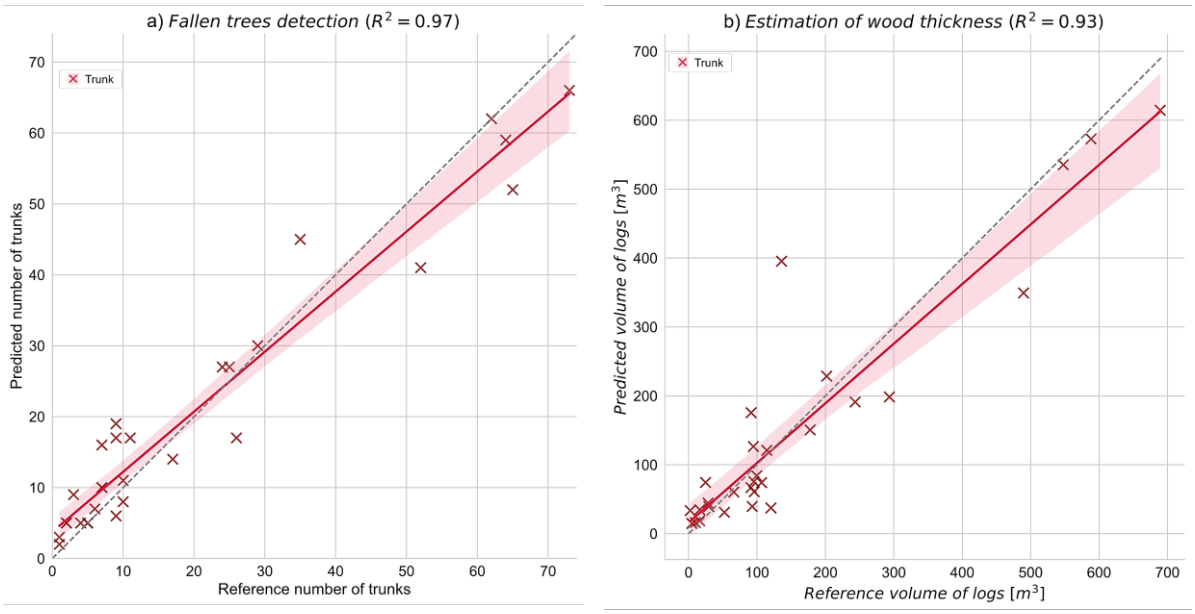

a) b)

Figure 4. a) Estimated log volume and b) Predicted number of logs. Each point on the scatter plot represents the number/volume of tree boles, calculated for each aerial image of the test area.

Source: own eleboration.

Table 2.
Mask R-CNN detection results. The model's effectiveness was calculated for variants with IoU (Intersection over Union) values of IoU = [0.1, 0.2, 0.3, 0.5], for the range of 0.1:0.5. Additionally, Precision, Recall, and F1-score values were computed at IoU ≥ 0.1.

AP_{10}	AP_{20}	AP_{30}	AP_{50}	AP_{10-50}	$Precision_{10}$	$Recall_{10}$	$F1-score_{10}$	N
0.522	0.427	0.312	0.118	0.418	0.795 ± 0.06	0.733 ± 0.08	$0.766 + 0.02$	32

Source: own eleboration.

The average value of the Precision metric is higher than the Recall (Table 2), indicating that, despite the model's strong performance in identifying wind-downed tree boles, it also tends to miss certain cases, rarely yielding false-positive errors. In developing the model, the key concern was to avoid missing any downed trees and prevent misidentification of leaning boles as standing trees. The Recall metric deviated by more than 2% from the average. The detection model's overall performance is expressed by the F1-score (reaching 0.766), as the harmonic mean of Precision and Recall. The model was evaluated using 32 test images. The average IoU value for the entire test dataset was 0.41±0.26. The standard deviation at 0.26 indicates a high degree of variability in the detection of downed tree logs. The maximum average value of IoU for a single image was 0.78. Out of the total instances, 75% fall below 0.61, and 50% below 0.41. The low AP for higher IoU thresholds indicates the model's low detection capabilities at low overlap criteria. High values of IoU overlap proved difficult to achieve, given the log small area, the numerous overlapping objects, and the narrow and irregular surface shape of uprooted or windsnapped trees. In small object detection, even slight differences between

the prediction and the reference can result in low Intersection over Union values. Given the above conditions, the results were analyzed in ranges lower than the typically analyzed range of 0.5-1.0. As the IoU_(10-50) threshold increases, the AP value decreases (-0.404). The model achieves its highest accuracy at low IoU overlap criteria. For overlap values between 0.1 and 0.5, the AP was 0.418. The highest AP (0.522) value within the IoU range analyzed reached an IoU threshold of 0.1.

Visual assessment

The nature of the tasks performed by the Mask R-CNN model also necessitates an evaluation of the decisions it makes, through a visually analysis of the nature of the errors it produces. This allows additional conclusions to be drawn regarding the errors.

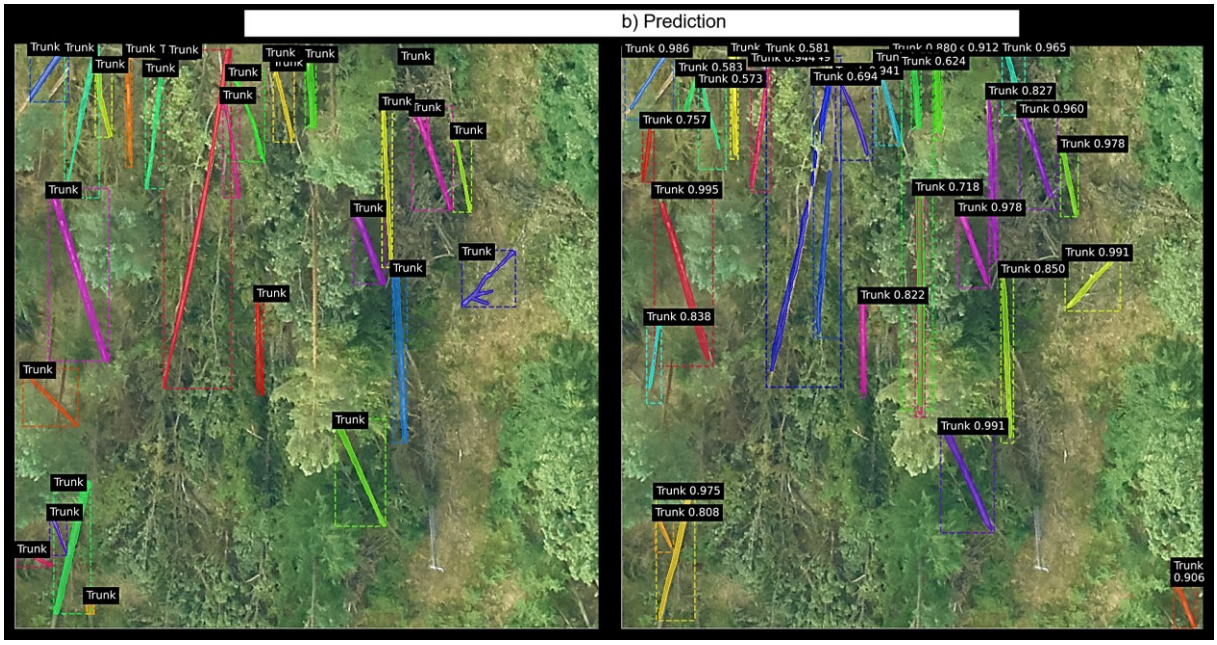

Figure 5. Prediction results. Apart from the mask and bounding box annotations, the illustration shows confidence scores for each indicated instance.

Source: own eleboration.

The model shows high sensitivity in identifying such objects as uprooted trees. Indication errors arise in the case of the tree boles partially obscured by neighboring tree branches. The continuity of tree log masking can be interrupted by obscurations from other objects (Figure 5).

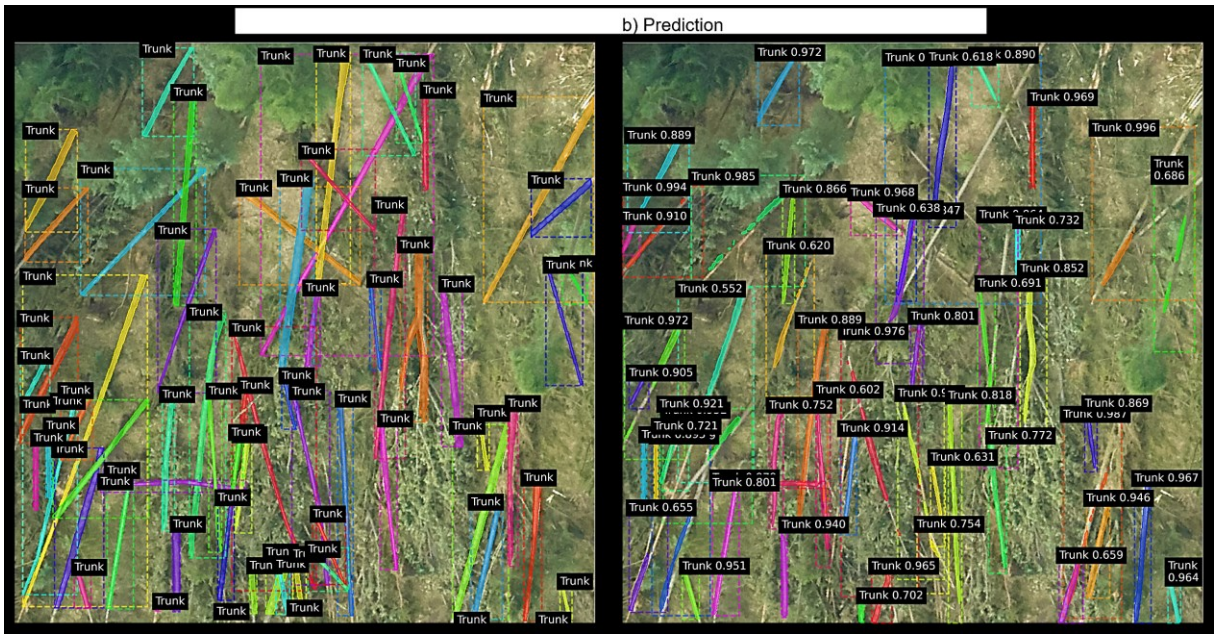

Figure. 6. Prediction results. The model is observed to encounter difficulties in accurate masking of very long tree boles extending beyond the image area.

Source: own eleboration.

The model remains capable to identifying individual boles, even under conditions of high density of downed trees. Strongly leaning, but not dead, trees are at high risk of misidentification as uprooted. The effectiveness of determining the extent and location of a dead tree is higher than that of an exact mask defining the extent of the bole (Figure 6).

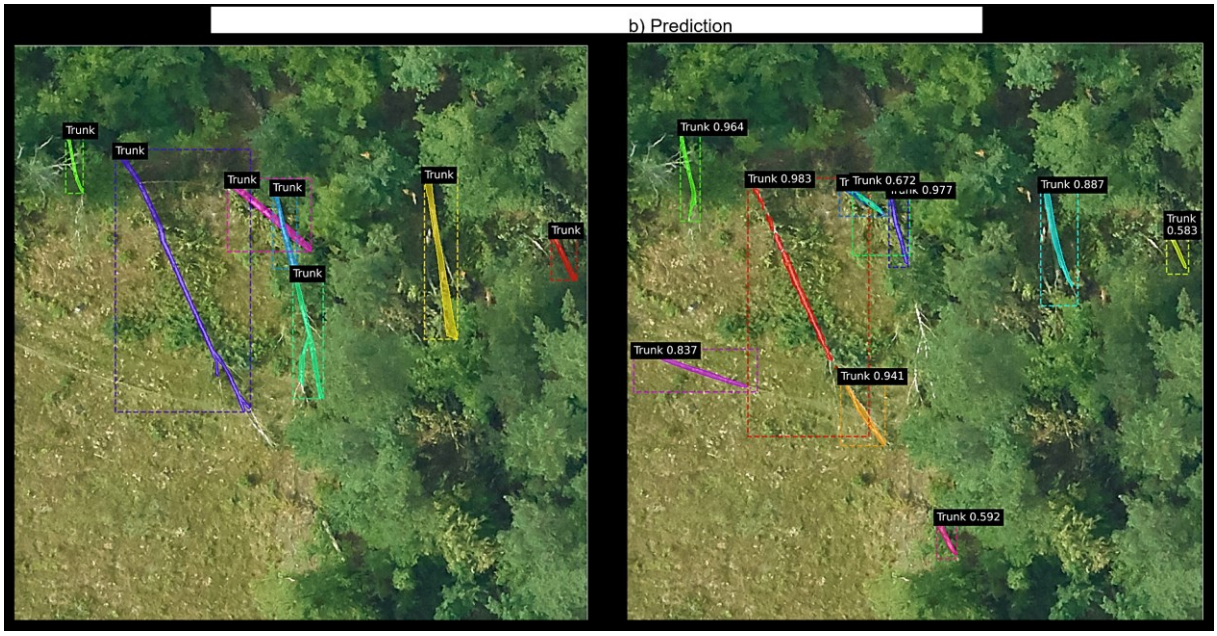

Figure 7. Prediction results. Whenever overlong logs are detected, the model splits the object into smaller parts, without omitting any segments of the identified log.

Source: own eleboration.

Despite the adjustment of the anchor scale parameter, to identify larger objects, the model was observed to continue to split longer logs into several parts (Figure 7). Perhaps the dataset representation needs to be extened to include examples of larger bole dimensions, especially in areas of higher uprooted tree density.

Estimation of potential revenue from timber sales

The log volumes calculated from the reference data and the predictions were summed and compared for the test area, the, taking several conditions into account (Table 3). Possible occurrence of two assortments and several common species was factored in. Based on the timber retail price list published by the Stare Jabłonki Forest District, potential timber sales revenue was estimated at the prices of the most economically viable species, such as pine, larch, spruce, beech, oak, and birch. The highest potential yield was calculated for a stand predominatly consisting of beech (533 PLN/m^3 net) or birch (482 PLN/m^3 net). The lowest prices were determined for larch (292 PLN/m^3 net) and spruce (305 PLN/m^3 net) (Przesław, 2023). The difference between the cumulative estimated and reference timber volumes totals 354 m^3 (Table 3).

Table 3.
Revenue estimation using timber volume predictions and unit prices for assortments S2A and S4.

Specie	Assortyment	Volume [m^3]	Net unit price [PLN]	Net price [PLN]	Value Added Tax [8%]	Gross price [PLN]
Pine	S2A	4961	316	1 567 676	125 414,08	1 693 090,08
		4607	316	1 455 812	116 464,96	1 572 276,96
Larch	S2A	4961	292	1 448 612	115 888,96	1 564 500,96
		4607	292	1 345 244	107 619,52	1 452 863,52
Spruce	S2A	4961	305	1 513 105	121 048,40	1 634 153,40
		4607	305	1 405 135	112 410,80	1 517 545,80
Beech	S2A	4961	533	2 644 213	211 537,04	2 855 750,04
		4607	533	2 455 531	196 442,48	2 651 973,48
Oak	S2A	4961	352	1 746 272	139 701,76	1 885 973,76
		4607	352	1 621 664	129 733,12	1 751 397,12
Birch	S2A	4961	482	2 391 202	191 296,16	2 582 498,16
		4607	482	2 220 574	177 645,92	2 398 219,92
Pine	S4	4961	125	620 125	49 610,00	669 735,00
		4607	125	575 875	46 070,00	621 945,00
Larch	S4	4961	115	570 515	45 641,20	616 156,20
		4607	115	529 805	42 384,40	572 189,40
Spruce	S4	4961	105	520 905	41 672,40	562 577,40
		4607	105	483 735	38 698,80	522 433,80
Beech	S4	4961	153	759 033	60 722,64	819 755,64
		4607	153	704 871	56 389,68	761 260,68
Oak	S4	4961	140	694 540	55 563,20	750 103,20
		4607	140	644 980	51 598,40	696 578,40
Birch	S4	4961	147	729 267	58 341,36	787 608,36
		4607	147	677 229	54 178,32	731 407,32

Source: own eleboration.

The usability of timber is determined through assortative classification. Grade S2A timber, used in the pulp and paper industry, can contain hard rot and insect galleries, but foreign bodies and charring are not acceptable. Grade S4 timber is intended for firewood use, thus foreign matter, charring and curvature are in this case acceptable. Firewood is subject to less stringent criteria requirements than industrial wood (Lewandowska-Gross & Stępień, 2013). The average difference between the estimated and the reference S2A assortment density is 145.281 PLN gross, and 50.02 PLN gross for the S4 assortment. The estimated revenue error totals 7.13%. Noteworthy are the large differences in the S2A and S4 assortment retail prices. The assortment-specific difference between the reference and the estimated gross revenue from pine is 950 331.96 PLN. Such significant differences lead to the conclusion that the key factor is the speed of logging operations in a given area, before the downed timber loses its industrial usability.

7. Discussion

Related works

The challenging issue of assessing forest damage caused by high-speed winds has been studied by various researchers. Artificial intelligence methods find application in post-disturbance crisis management (Xu et al., 2021). The methodologies employed entails certain limitations, however, which this study seeks to address and potentially remedy. The study involved the use of the Mask R-CNN convolutional neural network model to estimate the amount downed timber. Estimation of the extent of windstorm damage has already been attempted. Vasileios Linardos et al. expound in their work that the extent of post- disturbance damage is of crucial relevance to rapid rescue operations (Linardos et al., 2022). Using Landsat satellite imagery, windstorm-affected areas can be identified with up to 86% accuracy (Haidu et al., 2019). The level of detail in the satellite imagery analysis results is limited by the low spatial resolution of the images. Landsat data can be used to identify damage exceeding 0.5 hectares (Haidu et al., 2019). Smaller clusters of downed trees should not be ignored, as they potentially harbor unwanted species of insects and fungi (Einzmann et al., 2017). Similar results were obtained using the images recorded by the Sentinel-2 and Planet Scope satellite constellations (Dalponte et al., 2020). Images recorded by cameras attached to Unmanned Aerial Vehicles (UAV) are also used in post-disturbance area identification (Mokroš et al., 2017). The use of aerial imagery offers a clear advantage over satellite imagery, as it provides much more detailed information. The results obtained using Landsat satellite images were observed to be underestimated, compared to those obtained using aerial UAV images and ALS ground laser scanning. The estimate based on both types of data overestimated the actual

amount of timber by 4.93% (Mokroš et al., 2017). The design of our model began with exclusive use of aerial images, which can be integrated with other types of data in the future. Multi-temporal elevation data, such as Digital Surface Models (DSM), enable identification of damaged areas by calculating the differences in tree stand height. The extent of damage is determined based on these differences (Ivanova, Shashkov, 2022). Remote sensing methods, applied to monitor forest changes, employ three main approaches. The first is based on individual tree detection (ITD). The second - Object Based Image Analysis (OBIA) - involves analysis of grouped raster cells (objects). The third approach derives predictors from pixel-based analysis (PBA) of image values (Einzmann et al., 2017). As emphasized by Yanlei Feng et al., however, the drawback in monitoring methods based on optical images alone lies in the need to use images of the Earth's surface unobscured by cloud cover (Feng et al., 2023). Considering the above factors, the method offers the advantage of its applicability regardless of cloud cover. The solution described utilizes the post-disturbance data collected. Some solutions, however, utilize multi-temporal data, involving a comparison of data collected prior and after the onset of a windstorm. Using the ITD method and the terrestrial laser scanning data collected both prior to and after the windstorm event, the volume of timber can be estimated with an MPE error of: -10.6% (Onoszko et al., 2019). Based on the difference in vegetation intensity, damaged forest areas can be identified using the Normalized Difference Vegetation Index (NDVI). The use of high-resolution data allowed precise volume estimations in the selected area (Onoszko et al., 2019). The approach employed in a study by Kathrin Einzmann et al. necessitates the collection of data over two relevant periods - prior to and after the windstorm. The advantage satellite images offer lies in the use of additional infrared spectral channels and the generation of useful vegetation indices. Vegetation indices have been proven to enable the identification of windthrow areas (Einzmann et al., 2017). Satellite image resources allow such information to be collected over a broad window of time. One limitation lies in the frequency of image recordings of the same location. In crisis management, quick collection to data is of crucial significance. Dmitry E. Kislov et al. also proved that the extent of windstorm damage can be determined by convolutional neural network models utilizing high-resolution satellite images (Kislov, Korznikov, 2020). They classified windstorm-affected areas using the PBA approach, based on satellite images of 0.3-0.5 meter resolution. The overall accuracy of the naive Bayes classifier amounted to an F1 score of 0.79. Using two variations of the U-Net convolutional neural network, however, they obtained an F1 score ranging between 0.90 and 0.92 (Kislov et al., 2021). The authors emphasize that a model tailored to data of a specific resolution can yield underestimations when data of lower spatial resolution is used (Kislov et al., 2021). Fuzhou Duan has developed a pixel classification model for UAV aerial images. Using the Random Forests model, downed logs were identified with the accuracy of 94.48%. Highlighted pixels, corresponding to the windthrow logs, were analysed using the Hough Transform (Duan et al., 2017). The author stresses that the method is suitable for identifying slender-boled trees (Duan et al., 2017). Stefan Reder et al. employed a semantic

segmentation approach to identify downed logs. Using the U-Net convolutional neural network model, they obtained an F1-score of 75.6% (Reder et al., 2021). Although the benefits of using pre-trained models have been recognized, the approach can lead to longer inference times. The original images were split using the sliding window technique, with consecutive sections of the aerial image fed into the model, each section sized 256 x 256 pixels. Due to the longer inference time, however, the initial spatial resolution of 6.3 cm was reduced to 7 cm. The authors used image tiles sized 20 m x 20 m, corresponding to the 256 x 256 pixel grid at a GSD of 6.3 cm, and thus eliminated the need for the sliding window approach (Reder et al., 2021). In our study, we adhered to the conventional method of segmenting larger aerial images into smaller sections. The author emphasizes, nevertheless, that by preserving a high spatial resolution, the precision of calculations is maintained, at a simultaneous multiplication of the time needed for inference (Reder et al., 2021). The U-Net model was used in a study on the segmentation of individual tree boles. The model outputs a confidence map for raster pixel classification. Its output is transformed using the SAC function, which extracts individual logs from the mask. The study yielded high quality results. The Intersection over Union similarity between the prediction and the reference masks reached a range of 0.55-0.59, while the detection accuracy, in terms of completeness, ranged from 0.78 to 0.82 (Polewski et al., 2021). In a study by Nishant Jasiwal et al., volume estimates were derived from data collected during summer months. Worth mentioning is that wind disturbances are not exclusive to summer and can likewise occur in winter. Jasiwal's team formulated a model categorizing regions into five different types, one of which identifies windthrows. The model also detects regions of previous logging operations, although this particular study did not cover such cases. The aerial images used not only contained the RGB channels, but the near-infrared (NIR) channel as well. Jasiwal has emphasized that the DeepLabV3 model produced better results, as evidenced by the Intersection over Union score of 0.91. The study's applicability, however, lies primarily in the identification of potential damage zones (Jaiswal et al., 2022). Gherardo Chirici et al. employed the classic method of felled log area identification via Line Intersect Sampling in their study. The number of downed trees was estimated by multiplying the area affected by damage and the number of trees per hectare in that area. The volume was estimated based on pre-disaster tree bole height and diameter. The method also factors in species diversity, using existing Forest Inventory databases. The author has proposed a method for estimating the extent of losses, utilizing post-event ALS (Airborne Laser Scanning) data only (Chirici et al., 2018).

8. Conclusion

The present article describes a method characterized by low complexity. Its simplicity is evident in, for example, the type of data utilized. This low complexity also results in reduced aerial image processing time. The advantage of the proposed solution lies in the flexibility of data acquisition. The approach is based on the deployment of unmanned aerial vehicles (UAVs). The utilization of UAVs enables cost-effective aerial campaigns below cloud cover. As technology advances, the availability of these devices to forest managers continues to increase (Ecke et al., 2022). UAVs facilitate the acquisition of high-resolution data, which is particularly important when capturing imagery of terrain with variable topography or cloud cover, where alternative remote sensing methods encounter limitations (Zhang, Zhu, 2023). From a management perspective, the UAV-based approach demonstrates exceptional cost-effectiveness, achieving approximately 70% reduction in aerial survey expenses compared to conventional manned aircraft operations, while simultaneously providing on-demand deployment capabilities that align with dynamic business requirements. We anticipate that interest in artificial intelligence applications utilizing aerial photography will continue to expand. Previous investigations addressing wind damage extent assessment have also employed airborne laser scanning (ALS) data. However, the processing of LiDAR data necessitates substantially greater pre-processing effort. The proposed method enables damage localization at the individual tree level. A comprehensive dataset can be obtained through a single aerial survey. This single-survey requirement translates into significant operational efficiency gains, enabling forest managers to minimize operational downtime and expedite decision-making processes, thereby mitigating potential revenue losses associated with delayed timber salvage operations. Accuracy is maintained through, inter alia, the acquisition of imagery with a consistent spatial resolution of 4 cm. The standardized 4 cm resolution ensures consistent, auditable data quality that satisfies regulatory compliance requirements and facilitates transparent stakeholder communication, both of which are essential for maintaining business credibility and securing favorable insurance terms. Considering these aspects, the proposed method demonstrates clear advantages over previously described methodologies. The scalability of this method enables organizations to expand monitoring operations across multiple forest districts without proportional increases in technical personnel, thereby creating strategic advantages through centralized data processing and integrated management dashboards. For several reasons, further refinement of this solution is warranted to ensure its broadest possible application. The study reveals considerable potential for development; the approach can be enhanced through modifications to both the utilized data and the employed estimation methodologies. Implementation of this technology positions organizations as industry innovators, attracting premium clients and strategic partners while creating opportunities for novel service offerings and revenue streams within the rapidly expanding

forest management technology sector. Future improvements to detection capabilities are planned, including expansion of the training dataset size and incorporation of cases from additional forest districts. Dataset enrichment may include the integration of imagery captured during seasons other than summer. Currently, the model's effectiveness achieved during training can only be sustained when applied to data exhibiting characteristics similar to those of the training dataset. Enhancement of input data quality is planned through implementation of a two-stage verification protocol for the prepared reference data. This modification is expected to substantially improve the reliability of the obtained results. The method requires further validation based on field measurement temporal data. To minimize error, dataset enrichment through integration with satellite radar data represents a viable approach. More sophisticated volume calculation methods, based on the Smalian, Huber, or Newton formulae, warrant exploration in subsequent research phases (Mushar et al., 2020).

Acknowledgments

The study used utilized data provided by OPEGIEKA Sp. z o. o., located at Al. Tysiąclecia 11, 82-300 Elbląg. All calculations and experiments were carried out using the company’s infrastructure.

Competing interests

The authors have no relevant financial or non-financial interests to disclose.

9. Author contributions

All authors have contributed to the study conception and design. Material preparation, data collection and analysis were performed by Dominik Mielczarek, Krzysztof Najman. The first draft of the manuscript was written by Dominik Mielczarek and all authors commented on previous versions of the manuscript. All authors have read and approved the final manuscript.

References

1. Cheng, X, Dooshosseini, A., Kunkel, J. (2022). Improve the Deep Learning Models in Forestry Based on Explanations and Expertise. *Frontiers in Plant Science, Vol. 13*.
2. Chirici, G., Bottalico, F., Giannetti, F. et al. (2018). Assessing forest windthrow damage using single-date, post-event airborne laser scanning data. *Forestry*: *An International Journal of Forest Research, Vol. 91, Iss. 1,* pp. 27-37.
3. Dalponte, M., Marzini, S., Solano-Correa, Y. et al. (2020). Mapping forest windthrows using high spatial resolution multispectral satellite images. *International Journal of Applied Earth Observation and Geoinformation, Vol. 93, December*.
4. Dhubháin, A., Farrelly, N. (2018). Understanding and managing windthrow. *Silviculture/Management, No. 23*, pp. 1-4.
5. Diez, Y., Kentsch, S., Fukuda, M. et al. (2021). Deep learning in forestry using UAV-acquired RGB data: A practical review. *Remote Sensing. Vol. 13, Iss. 14*, 2837.
6. Dmyterko, E., Bruchwald, A. (2020). Assessment of damages in Polish forests caused by the hurricane in August 2017. *Sylwan, Vol. 164, Iss. 5*, pp. 355-364.
7. Dmyterko, E., Mionskowsk, M., Bruchwald, A. (2015). Risk of the wind damage to the forests in Poland on the basis of a stand damage risk model. *Sylwan, Vol. 159, Iss. 5,* pp. 361-371.
8. Duan, F., Wan, Y., Deng, L. (2017). A Novel Approach for Coarse-to-Fine Windthrown Tree Extraction Based on Unmanned Aerial Vehicle Images. *Remote Sensing, Vol. 9, Iss. 4,* 306.
9. Ecke, S., Dempewolf, J., Frey, J. et al. (2022). UAV-Based Forest Health Monitoring: A Systematic Review. *Forest Remote Sensing, Vol. 14, Iss. 13*, 3205.
10. Einzmann, K., Immitzer, M., Böck, S. et al. (2017). Windthrow Detection in European Forests with Very High-Resolution Optical Data. *Forests, Vol. 8, Iss. 1*, 21.
11. Feng, Y., Negrón-Juárez, R., Romps, D., Chambers, J. (2023). Amazon windthrow disturbances are likely to increase with storm frequency under global warming. *Nature Communications, Vol. 14. Iss. 1,* 101.
12. Filotas, E., Parrot, L., Burton, P., Chazdon, R., Coates, K., Coll, L., Haeussler, S., Martin, K., Nocentini, S., Puettmann, K. et al. (2014). Viewing forests through the lens of complex systems science. *Ecosphere, Vol. 5, Iss. 1*, pp. 1-23.
13. Gardiner, B., Quine, C. (2020). Management of forests to reduce the risk of abiotic damage - A review with particular reference to the effects of strong winds. *Forest Ecology and Management. Vol. 135, Iss. 1*, pp. 261-277.
14. Gardiner, B., Schuck, A., Schelhaas, M., Orazio, C., Blennow, K., Nicoll, B. (eds.) (2013). *Living with Storm Damage to Forests*. European Forest Institute.

15. Gieralowiec, K. (2020). *Influence of timber harvesting technology on changes in utility value of wood from post-hurricane areas*.
16. Goodfellow, I., Bengio, Y., Courville, A. (2018). *Deep Learning*. PWN.
17. Haidu, I., Furtuna, P., Lebaut, S. (2019). Detection of old scattered windthrow using low cost resources. The case of Storm Xynthia in the Vosges Mountains, 28 February 2010. *Open Geosciences*, *Vol. 11, Iss. 1*, pp. 492-504.
18. Hastie, T., Tibshirani, R., Friedman, J. (2001). *The Elements of Statistical Learning*. Stanford: Springer.
19. He, K., Gkioxari, G., Dollar, P., Girshick, R. (2017). *Mask R-CNN*. Proc IEEE International Conference on Computer Vision (ICCV). Venice, Italy, pp. 2961-2969.
20. He, K., Zhang, X., Ren, S., Sun, J. (2015). *Deep Residual Learning for Image Recognition. arXiv.* Conference: 2016 IEEE Conference on Computer Vision and Pattern Recognition (CVPR). Las Vegas, 27-30 June, pp. 770-778.
21. Heinonen, T., Pukkala, T., Ikonen, V. (2009). Integrating the risk of wind damage into forest planning. *Forest Ecology Management, Vol. 258, Iss. 7,* pp. 1567-1577.
22. Ivanova, N., Shashkov, M. (2022). Tree stand assessment before and after windthrow based on open-access biodiversity data and aerial photography. *Nature Conservation Research, Vol. 7, Suppl. 1*.
23. Jaiswal, N., Bucher, T., Seiler, J. et al. (2022). Deep learning based windthrow detection for winter storms. In: *Remote Sensing for Agriculture, Ecosystems, and Hydrology, XXIV*. SPIE Sensors + Imaging 2022 (Remote Sensing).
24. Karra, K., Kontgis, C., Statman-Weil, Z. et al. (2021). *Global land use/land cover with Sentinel 2 and deep learning.* Conference: IGARSS 2021 - 2021 IEEE International Geoscience and Remote Sensing Symposium IGARSS. Brussels, 11-16 July 2021, 4704-4707.
25. Kislov, D., Korznikov, K. (2020). Automatic Windthrow Detection Using Very-High-Resolution Satellite Imagery and Deep Learning. *Remote Sensing, Vol. 12, Iss. 7*, 1145.
26. Kislov, D., Korznikov, K., Altman, J., Vozmishcheva, A., Krestov, P. (2021). Extending deep learning approaches for forest disturbance segmentation on very high-resolution satellite images. *Remote Sensing in Ecology Conservation, Vol.7, Iss. 3*, pp. 355-368.
27. Krisans, O., Samariks, V., Donis, J., Jansons, A. (2020). Structural Root-Plate Characteristics of Wind-Thrown Norway Spruce in Hemiboreal Forests of Latvia. *Forests, Vol. 11, Iss. 11,* 1143.
28. Kühmaier, M., Gollob, C., Nothdurft, A. et al. (2022). Capacity Planning of Timber Harvesting in Windthrow Areas. *Forests*, *Vol. 13, Iss. 2,* 350.
29. Lewandowska-Gross, M., Stępień, E. (2013). Changes of assortment structure of Scots pine stands of Ist site index class in Pisz Forest District. *Sylwan, Vol. 157, Iss. 6*, pp. 412-418.
30. Lin, T., Maire, M., Belongie, S. et al. (2014). *Microsoft COCO: Common Objects in Context.* Computer Vision – ECCV, pp. 740-755.

31. Linardos, V., Drakaki, M., Tzionas, P., Karnavas, Y. (2022). Machine Learning in Disaster Management: Recent Developments in Methods and Applications. *Machine Learning & Knowledge Extraction, Vol. 4, Iss. 2*, pp. 446-473.
32. Lindner, M., Maroschek, M., Netherer, S. et al. (2010). Climate change impacts, adaptive capacity, and vulnerability of European forest ecosystems. *Forest Ecology Management*, *Vol. 259, Iss. 4*, pp. 698-709.
33. Messier, C., Bauhus, J., Doyon, F., Maure, F., Sousa-Silva, R., Nolet, P., Mina, M., Aquilue, N., Fortin, M., Puettmann, K. (2019). The functional complex network approach to foster forest resilience to global changes. *Forest Ecosystems, Vol. 6*, pp. 6-21.
34. Mitchell, S. (1995). The windthrow triangle: A relative windthrow hazard assessment procedure for forest managers. *The Forestry Chronicle*, *Vol. 71, Iss. 4,* pp. 446-450.
35. Mokroš, M., Výbošťok, J., Merganiˇc, J. et al. (2017). Early Stage Forest Windthrow Estimation Based on Unmanned Aircraft System Imagery. *Forests*, *Vol. 8, Iss. 9,* 306.
36. Mushar, S., Ahmad, S., Shari, N., Kasmin, F. (2020) A comparative study of log volume estimation by using statistical method. *Journal of Science, Mathematics and Technology, Vol. 7, Iss. 1*, pp. 22-28.
37. O'Shea, K., Nash, R. (2015). *An Introduction to Convolutional Neural Networks*. Published in ArXiv.org 26 November.
38. Office of Forest Management and Forest Geodesy (2020). *Guidelines for conducting a large-scale forest status survey*.
39. Onoszko, K., Hawryło, P., Krawczyk, J., Mielczarek, D. (2019). *Inventory of post-hurricane damage in forest stands using multi-source remote sensing imagery: A case study of the Stare Jabłonki Forest District.*
40. Pi, Y., Nath, N., Behzadan, A. (2020). Convolutional neural networks for object detection in aerial imagery for disaster response and recovery. *Advanced Engineering Informatics, Vol. 43, Iss. C,* 101009.
41. Polewski, P., Shelton, J., Yao, W., Heurich, M. (2021). Instance segmentation of fallen trees in aerial color infrared imagery using active multi-contour evolution with fully convolutional network-based intensity priors. *ISPRS Journal of Photogrammetry Remote Sensing, Vol. 178,* pp. 297-313.
42. Pravalie, R., Niculita, M., Rosca, B. et al. (2023). Modelling forest biomass dynamics in relation to climate change in Romania using complex data and machine learning algorithms. *Stochastic Environmental Research and Risk Assessment*, *Vol. 37, Iss. 5,* pp. 1669-1695.
43. Reder, S., Mund, J., Albert, N. et al. (2021). Detection of Windthrown Tree Stems on UAV-Orthomosaics Using U-Net Convolutional Networks. *Remote Sensing, Vol. 14, Iss. 1,* 75.
44. Seidl, R., Schelhass, M., Rammer, W., Verker, P. (2014). Increasing forest disturbances in Europe and their impact on carbon storage. *Nature Climate Change, Vol. 4,* pp. 806-810.
45. Stąpor, K. (2011). *Object classification methods in computer vision*. Warszawa: PWN.

46. Sun, W., Bocchini, P., Davison, B. (2020). Applications of artificial intelligence for disaster management. *Natural Hazards: Journal of the International Society for the Prevention and Mitigation of Natural Hazards, Vol. 103, Iss. 3.* Springer, pp. 2631-2689.
47. Tampekis, S., Kantarzis, A., Arabtzis, G. et al. (2024). Conceptualizing Forest Operations Planning and Management Using Principles of Functional Complex Systems Science to Increase the Forest's Ability to Withstand Climate Change. *Land, Vol. 1, Iss. 2*, 217.
48. Valinger, E., Fridman, J. (2021). Factors affecting the probability of windthrow at stand level as a result of Gudrun winter storm in southern Sweden. *Forest Ecology and Management*, *Vol. 262*, pp. 398-403.
49. Walker, B., Holling, C., Carpenter, S., Kinzig, A. (2004). Resilience, adaptability and transformability in social-ecological systems. *Ecology and Society, Vol. 9, Iss. 2, Art. 5*.
50. Xu, Y., Liu, X., Cao, X. et al. (2021). Artificial intelligence: A powerful paradigm for scientific research. *The Innovation*, *Vol. 2, Iss. 4,* 100179.
51. Zachara, T. (2006) Damage to forests caused by snow and wind and the ways of counteracting it. *Sylwan, Vol. 150, Iss. 10*, pp. 54-64.
52. Zhang, Q., Xu, J., Xu, L., Guo, H. (2016). *Deep Convolutional Neural Networks for Forest Fire Detection.* In: International Forum on Management, Education and Information Technology Application, (IFMEITA 2016). pp. 568-575.
53. Zhang, T., Suen, C. (1984). A Fast Parallel Algorithm for Thinning Digital Patterns. *Communications of the ACM, Vol. 27, Iss. 3*, pp. 236-239.
54. Zhang, Z., Zhu, L. (2023). A review of methods for high-resolution UAV mapping. *Drones, 151*, pp. 132-143.
55. Zhu, M. (2004). *Recall, precision and average precision*. Technical Report, University of Waterloo.